J Mater Sci: Mater Med (2006) 17:1079–1087
DOI 10.1007/s10856-006-0534-7

Crystallinity in apatites: how can a truly disordered fraction be distinguished from nanosize crystalline domains?

Giancarlo Celotti · Anna Tampieri · Simone Sprio · Elena Landi · Luca Bertinetti · Gianmario Martra · Caterina Ducati

Received: 4 July 2005 / Accepted: 24 October 2005

Abstract In the last decade synthetic apatites mimicking the human natural one have been widely prepared and characterized from the physico-chemical point of view; however a shading zone is still remaining related to the evaluation and distinction of the less crystalline part, almost amorphous, and the crystallographically well ordered, nano-sized part, inside the apatite itself. Actually natural apatite forming bone tissue can include both types of crystals whose prevalence is dependent from the specific bone evolution stage and the specialized tissue performance. The quantitative description of such a combination usually represents a puzzling problem, but the result can also clarify the definition of "crystallinity in apatite" that appears still controversial. Many different synthetic apatites, including those nucleated on organic templates, were analyzed with different techniques (X-ray diffraction, transmission electron microscopy, and so on) to clarify the true nature of the disordered part. The results, manipulated by the classical methodologies devised for substances with highly perturbed structural order, led to establish that only specifically prepared amorphous calcium phosphate is really a glass, while the distorted portion coexisting with more or less crystalline regions is simply nanocrystalline. Moreover, at the conceptual limit of crystallinity tending to zero, the two models surprisingly cease to be conflicting.

G. Celotti · A. Tampieri · S. Sprio (✉) · E. Landi
Institute of Science and Technology for Ceramics, ISTEC-CNR, Faenza, Italy

L. Bertinetti · G. Martra
Chemistry Department, University of Turin, Italy

C. Ducati
Department of Materials Science and Metallurgy, University of Cambridge, UK

Introduction

Increasing the interest in bioresorbable bioactive materials as bone substitute, much activity has been devoted to the design and synthesis of biomimetic apatites i.e. hydroxyapatites (HA) which mimic the composition (and thus the features) of natural bone intended as a dynamic system in equilibrium with a complex environment [1–4]. For this reason different kind of anionic and cationic substitutions have been performed raising the chemical similarity with bone and simultaneously causing distortion in the HA cell structure and/or affecting the crystallites formation, growth and morphology [5].

It is already well known that mineral component of bone has well defined features in relation to bone tissue function and age: in particular crystallinity degree and crystal size are related to a specific osteogenetic stage and ultimately to the bone biomechanic performance [6, 7]. For this reason it seems crucial to define the actual state of synthetic apatite, i.e. to gather information upon the disputed question connected to HA crystallinity degree which mingles and shades into nano-dimension of crystal domains.

The concept of crystallinity in matter, even if apparently well defined as the crystalline volume fraction of a phase in a sample, is a matter for discussion mainly when we are treating cases of very small or vanishing amounts. At the side of high crystallinity values, with long-range order almost unperturbed, when the situation tends to single crystal or large crystallites with small zones of intergranular transition (grain boundaries), there is little room for doubt: the high and well defined diffraction peaks turn out to be even too narrow for reliable crystallite size determination via the Scherrer equation.

The troubles arise from the opposite side, i.e. crystallinity very low or tending to zero, as usually occurring in biologic systems. The diffraction lines appear so broadened as to lose

Table 1 Main preparative features of the different HA powders

HA powder*	Synthesis conditions
Stoichiometric HA	$T = 25$ (low crystallinity) -40°C (medium crystallinity)
B-carbonated HA	$NaHCO_3$ as a carbonate source; $T = 40^{\circ}$C
Mg-doped HA	$MgCl_2 \cdot 6H_2O$ as a Mg source; $T = 40^{\circ}$C
HA nucleated on collagen fibres	Synthesis in an aqueous solution of self-assembling collagen fibres; $T = 25^{\circ}$C

* The reagents used were calcium hydroxide and orthophosphoric acid.

the shape of true peaks, becoming more and more similar to unresolved large humps.

However, there are two intrinsically different situations that can yield such an effect: (a) exceedingly small but well-ordered crystallites or (b) really amorphous matter (retaining only short-range order at the scale of few atomic neighbours), that we can call conventionally "nanocrystals" and "glass" respectively.

Moreover, it has to be noted that new materials are being discovered that lie between the two extremes: they have a well-defined structure over the local and intermediate range that can be described rather well by a small unit cell and a relatively small number of parameters. However, they are not long-range ordered and the structural coherence dies out on a nanometer length scale: these materials are often called nanocrystals. It should be emphasised that this definition of nanocrystals goes beyond perfect crystals that are simply very small (nanometer in size) and includes materials where the particle size can be larger but the structural coherence is nanometer length scale. Another class of interesting materials was found where long-range order exists but significant structural distortions are also present that are not reflected in the average structure.

It is easy to understand that the "simple" concept of crystallinity shows rather complicated aspects and subtle distinctions deserving careful investigation.

It is to cast some light onto this intriguing dilemma that we analyzed in depth the diffraction data from many synthetic hydroxyapatites, encountered over years of research in the field of biomimetic ceramic materials [8].

Experimental

Hundreds of X-ray diffraction (XRD) powder patterns from various synthetic HA were compared and studied; in particular we focused our attention on perturbed order samples: (a) pure HA prepared by traditional wet methods at different (low) temperatures with final low and medium crystallinity; (b) carbonated HA (CHA), mainly in B position; (c) Mg-doped HA and CHA; (d) HA directly nucleated on self-assembling collagen fibres. The details of preparation and physico-chemical characterisations are reported elsewhere [9–13] and summarized in Table 1.

Moreover, specially for the present work, we prepared amorphous calcium phosphate (ACP) starting from $Ca(NO_3)_2 \cdot 2H_2O$, $Na_2HPO_4 \cdot 2H_2O$, $Na_4P_2O_7$ and NaOH, then washing the product in NH_4OH in agreement with the procedure proposed by LeGeros [14, 15], and largely varying the concentration of $Na_4P_2O_7$ (PO_4/P_2O_7 ratio from 4 to 40) that can be considered an effective inhibitor of HA crystallisation. The Ca/P molar ratio was varied too between 1.50 and 1.67 with practically undetectable effects. On the other hand the powders with PO_4/P_2O_7 up to 10 can be considered representative of true amorphous Ca phosphate, while when this ratio exceeds 10 the crystallisation of HA begins yielding various degrees of low crystallinity HA.

The XRD patterns of the most significant powders in these two categories were carefully recorded (Siemens D-500 diffractometer, CuKα radiation, angular range from 10 to 150°, step width 0.04° counting time 5 s). The data, after proper corrections, were analysed by the method originally proposed for amorphous substances by Warren [16] and recently upgraded by Egami and Billinge [17] to obtain the pair distribution function (PDF) or radial atomic distribution (RAD) characterising the short-range order: in some cases the so-called "amorphous contribution" subtended under the surviving crystalline peaks was graphically outlined and separately analysed.

Even if the maximum recorded value of $s = 4\pi \sin\theta/\lambda$ was only about 8 A^{-1}, satisfactory results were obtained due to the sufficiently rapid convergence of experimental intensity (converted in absolute units) to the calculated total independent scattering free of interference effects.

Simulations of the XRD patterns as modified by nanometer scale of crystallite dimension (0.5–2 nm) for the main Ca phosphates were calculated using the Powder Cell 2.1 programme.

To control the thermal stability, thermo-gravimetric/thermo-differential analysis (TG-DTA: Polymer STA 1500) of representative samples was performed in the room temperature-1400°C range.

Fourier-Transform Infrared spectroscopic analysis (FTIR: Thermo-Nicolet Avatar) was carried out as well to identify possible differences and to have an idea of the unintentional degree of carbonation in the samples.

Observations of some selected powders by transmission electron microscopy (TEM) were performed with a JEOL

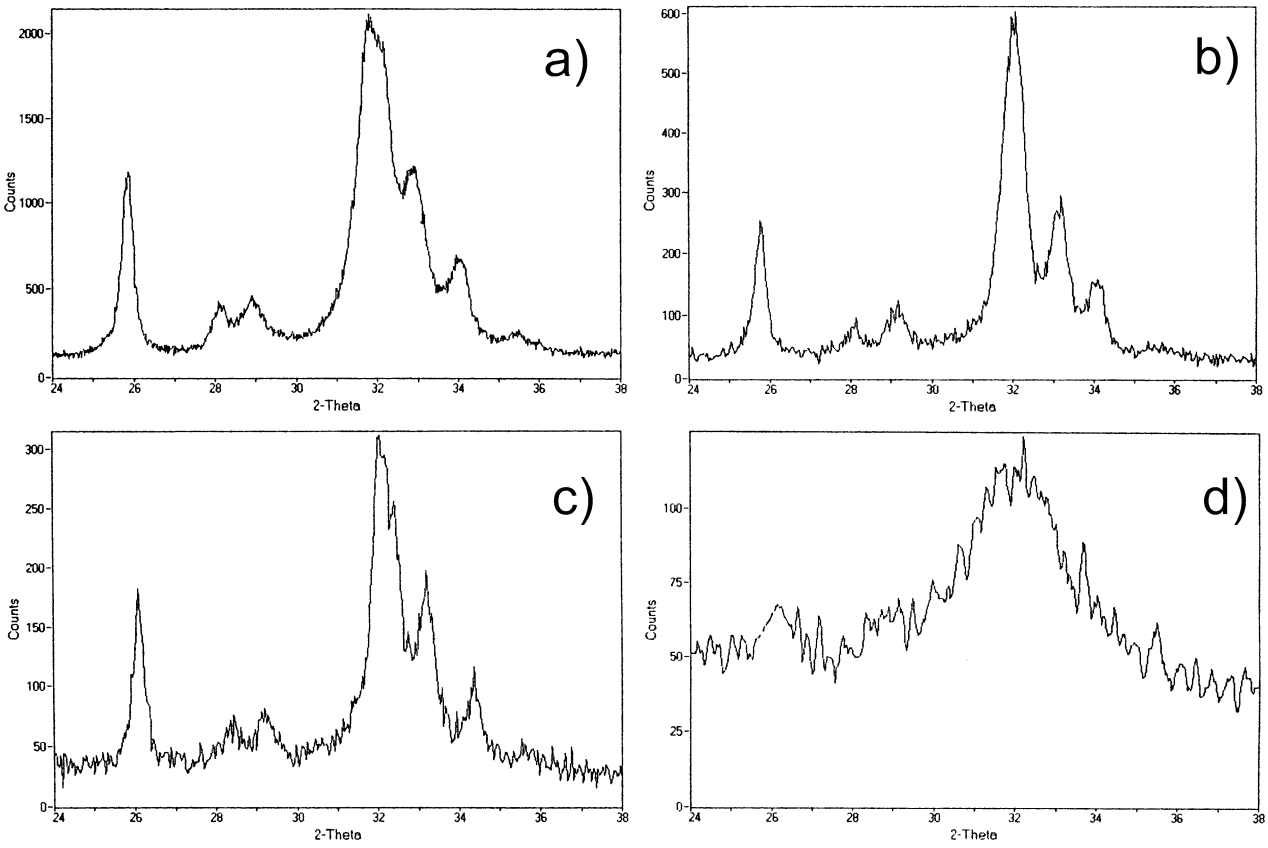

Fig. 1 Typical XRD patterns of different representative HA samples: (a) low crystallinity HA; (b) mainly B position carbonated HA (CHA); (c) Mg doped HA; (d) HA directly nucleated on self-assembling collagen fibres.

EX4000 instrument with acceleration potential of 400 kV. Samples were dispersed on lacy carbon Cu grids by contact with the grids and subsequent gentle shaking.

Results and discussion

Figure 1 displays typical XRD patterns representative of the four classes of HA samples listed at the beginning of the previous section that are the object of our studies: it is easy to see that they refer to very different degrees of structural order. When HA is directly nucleated on collagen fibres it is hard to recognise even the main ones of its well known powder diffraction features.

The XRD pattern for specifically prepared ACP is reported in Fig. 2, while that obtained as "amorphous background" by eliminating the residual crystalline peaks [18] from a low crystallinity HA pattern (LCB) is shown in Fig. 3: it is easy to see that the first presents much fewer interference effects, furthermore extending over a reduced angular range. The corresponding RAD curves, with and without the contribution of the average atomic density, are displayed in Figs. 4a,b and 5a,b respectively. It has to be remembered that some attempts to evaluate the crystalline HA to amorphous calcium phosphate ratio by an empirical simplified method very similar to those practised in polymer science were performed for

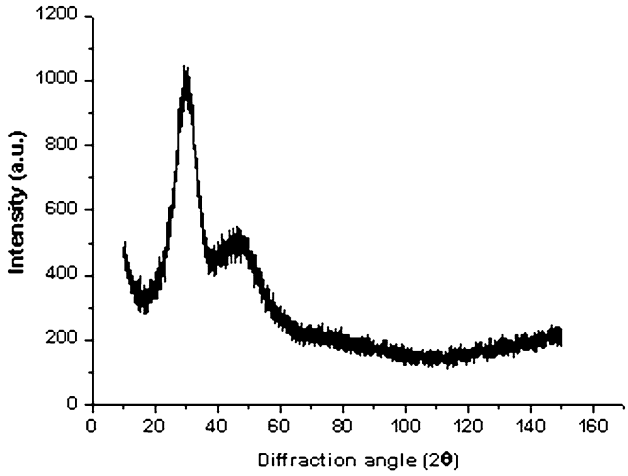

Fig. 2 XRD pattern for specifically synthesized ACP.

plasma-sprayed coatings, but the "amorphous" contribution was limited to the first hump between 24 and 36° of 2θ: in any case, the procedure is satisfactory to supply a sort of numerical figure of merit without structural implications [19].

The only attempt to evaluate in depth the characteristics of ACP in comparison with those of crystalline and variously perturbed HA remains the fundamental one of Posner and co-workers [20] dating 30 years ago, whose conclusions were: synthetic ACP is different from HA in stoichiometry,

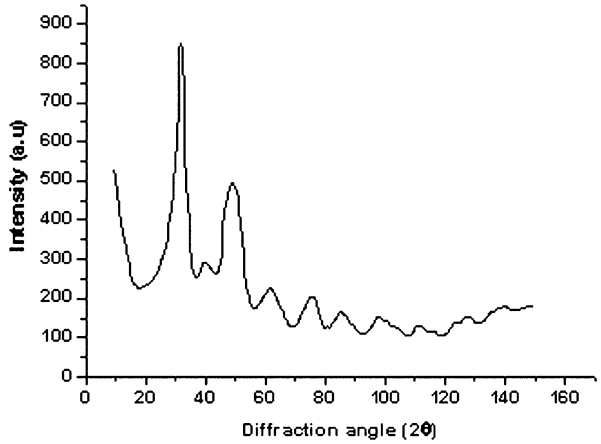

Fig. 3 XRD pattern obtained from a low crystallinity HA sample after careful elimination of residual crystalline peaks (LCB).

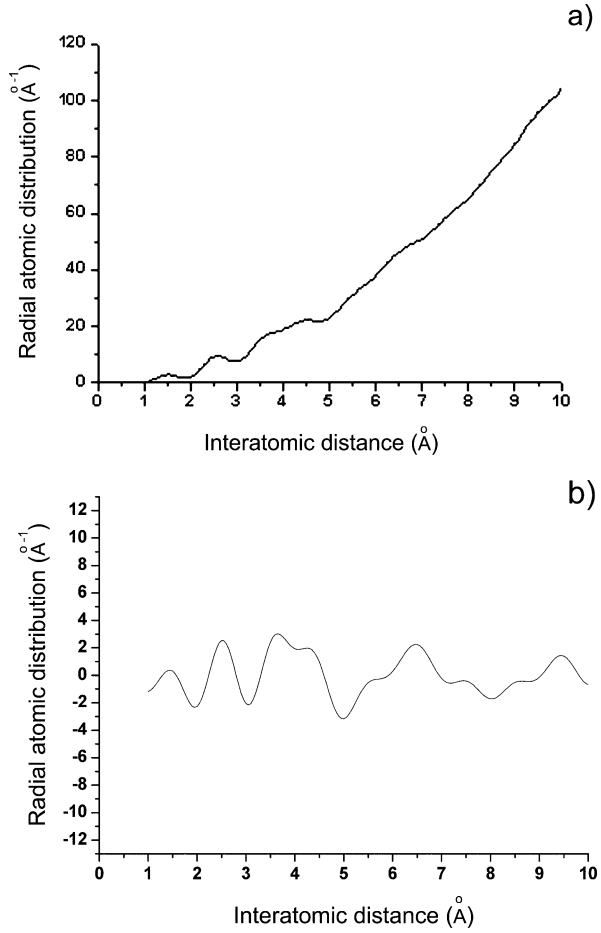

Fig. 4 RAD curves for ACP: (a) with and (b) without the contribution of the average atomic density.

does not consist of extremely small crystals of HA and has a distinctive radial distribution function from which the now famous structural model of spherical clusters about 10 Å in diameter was proposed.

To cope with the problem of different species present in the structure, an average atomic scattering factor calculated according to the molar concentrations was employed throughout.

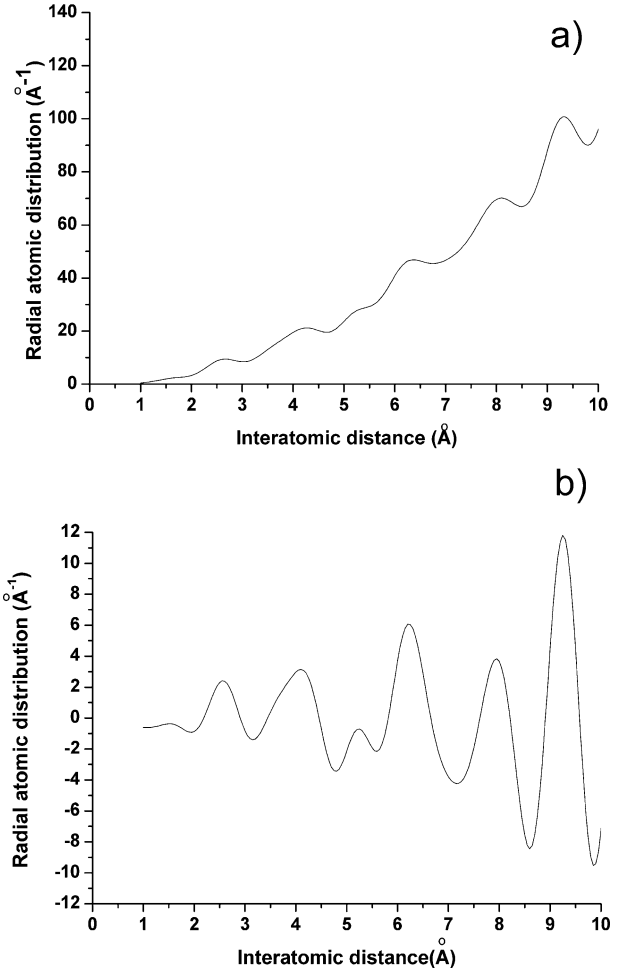

Fig. 5 RAD curves for LCB: (a) with and (b) without the contribution of the average atomic density.

The first gross feature appears to be the much greater smoothness of the ACP curves compared with the LCB ones; this indicates that the atomic distribution is less rigid and more difficult to quantify.

The interatomic distances after the first three ($r > 0.35$ nm) tend to be sensibly longer in ACP and for $r > 0.70$ nm it becomes difficult to find a sure biunivocal correspondence: clearly there is a loosening of the structural organisation in respect of LCB whose effects increase with distance.

While more and more distinct maxima are found in LCB at high r values, in ACP this trend appears reversed, indicating that the larger shells are broadened and widely undefined, due to the multitude of fairly different distances each with small number of atoms.

Another meaningful distinctive feature is the sequence (with only one negligible exception at low r) of regularly growing maxima with increasing r in ACP, typical of an almost statistically homogeneous atomic spatial distribution:

this is one of the most prominent characteristics of glasses and is not found in LCB that seems to still preserve a certain amount of anisotropic lattice constraints.

The behaviour of the peak representing the shortest distance (about 0.15 nm), that corresponds to P-O (and vice versa) in the PO_4 tetrahedron is interesting: it appears slightly sharper in ACP than in LCB. Even if it is well known that the low r region is affected by many mathematical errors, the observed feature could be linked to the higher repetitiveness of the PO_4 tetrahedra in a highly disordered structure in which they represent the only atomic group certainly maintaining its shape with limited dimensional fluctuations.

Considering all the atomic species as equivalent (an approximation that was also used in the RAD calculations for polyatomic compounds: see above), in HA every "average atom" occupies $528.8/44 = 12$ Å^3: this can be considered as a reference value to estimate if the RAD curves point towards thicker or thinner structural packings. In a spherical shell of minimum radius 1 Å and maximum 10 Å (volume about 4185 Å^3 corresponding to nearly 8 elementary cells of HA) we find 348 atoms on average: the sum of the areas of all the peaks in the RAD curves with the term $4\pi r^2 \rho_o$ added [17], considering them as Gaussian and taking care to avoid counting the overlapping sections more than once, gives a number to be compared with this value. As shown in Fig. 6a,b for ACP we obtain about

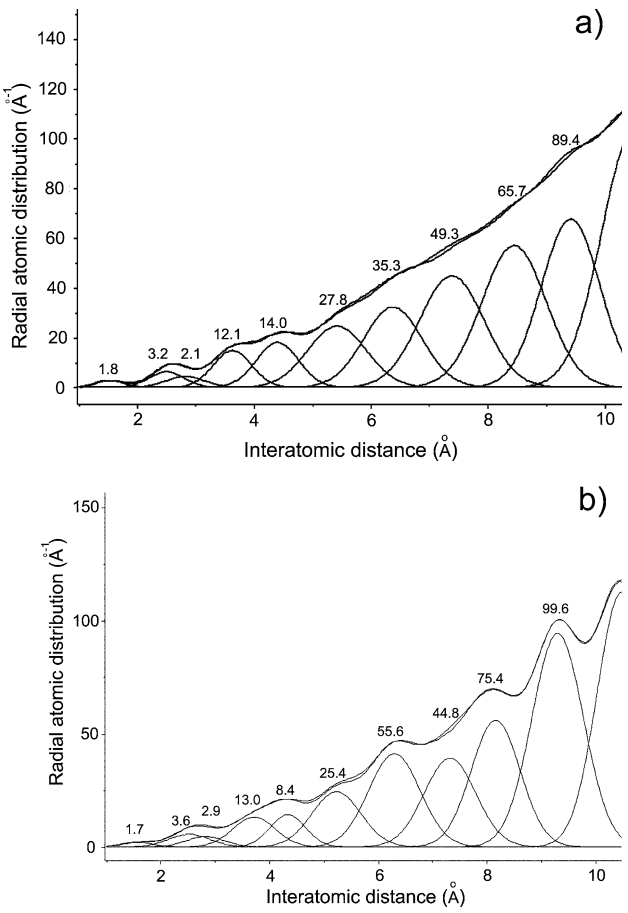

Fig. 6 RAD curves with evidenced the interatomic distance peaks forming the envelope: (a) for ACP; (b) for LCB. The reported numbers indicate how many "average" atoms are present in each spherical shell.

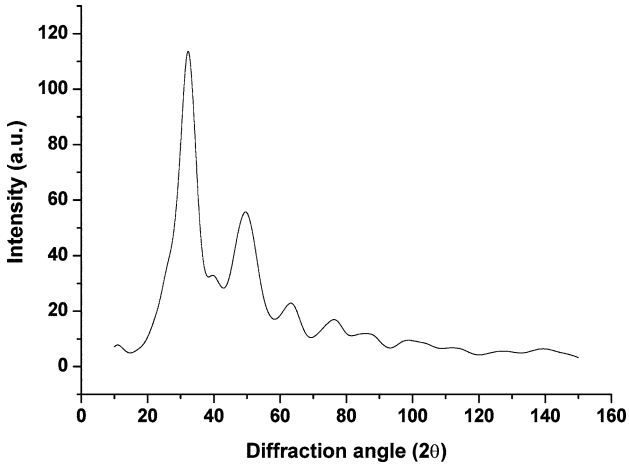

Fig. 7 Simulated XRD pattern for HA structured nanocrystals of size 1.5–2.5 nm.

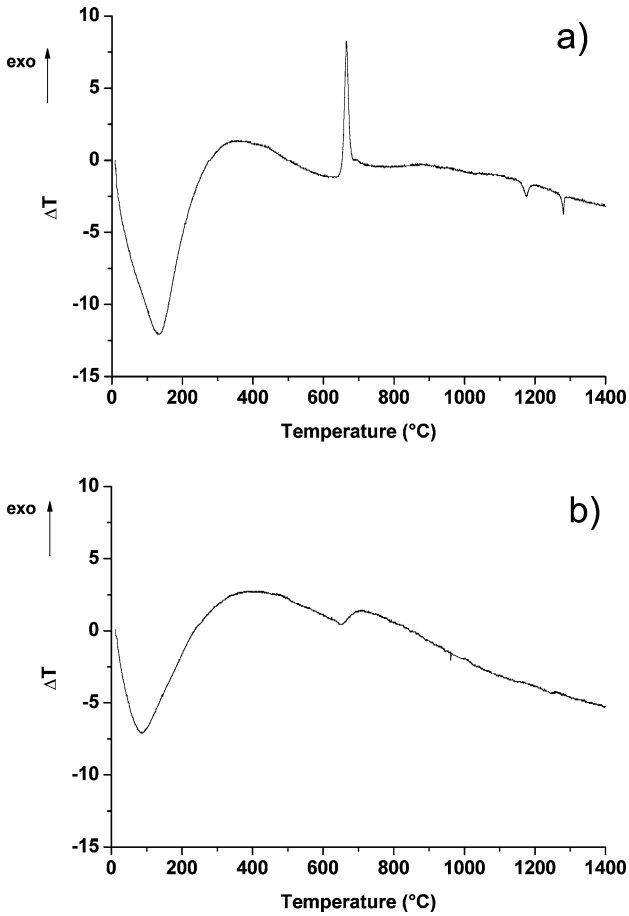

Fig. 8 DTA curves for: (a) ACP; (b) LCB.

300 (86%), while for LCB we have 330 (95%): both values are significantly lower, as expected, than in crystalline HA, but ACP is characterised by a less tightly packed arrangement.

From all the previous considerations, it is possible to assert with reasonable confidence that ACP is really an amorphous Ca phosphate, while LCB (which usually constitutes the non-crystalline back-ground in Ca phosphate samples) is more likely describable as a nanocrystalline fraction with crystallites of 1.5–2.5 nm (see the correspondent simulated XRD pattern in Fig. 7): these two situations present marked analogies only up to $r = 0.35$ nm, while beyond the intrinsically different atomic arrangements appear clearly established. It is worth mentioning that a reasonable reproduction of the XRD pattern of ACP can be obtained with a nanocrystalline model with the very small crystallite size of 0.8–1.3 nm: the only detail that cannot obviously be simulated by nanocrystalline models is the remarkable small angle scattering, which has a physically different origin and is always present when dealing with disordered structures characterized by considerable large-scale (5–50 nm) fluctuations in the electron density. Not even to be said that crystallites of size very similar to

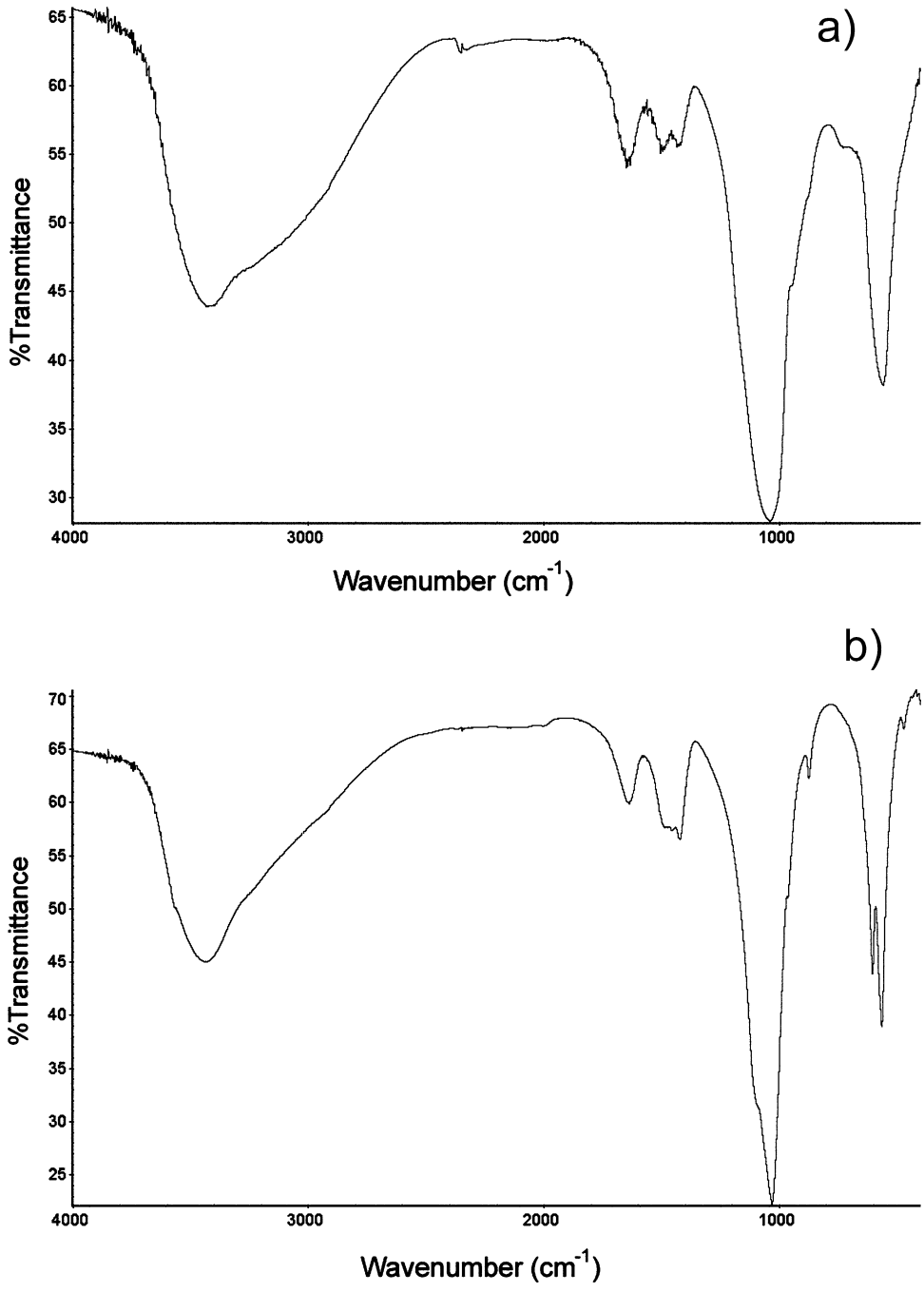

Fig. 9 FTIR spectra relative to: (a) ACP; (b) LCB.

that of the HA unit cell can hardly be considered as making sense at all.

Worthwhile to mention the fact that truly amorphous samples present in DTA curves (see Fig. 8) a sharp exothermic transition at about 665°C, corresponding to crystallisation (the phase formed is low-temperature α-TCP, an uncommon metastable modification formerly called $\bar{\alpha}$ and afterwards γ [21], characterised by an XRD pattern very similar to that of stable high-temperature α-TCP): this feature is completely absent from the DTA curves of nanocrystalline samples that remain HA (with a few percent of α-TCP) up to 1400°C, with almost complete crystalline fraction and crystallite size raised to 50–70 nm. Such an exothermic peak turns out to be a good indicator for distinguishing between amorphous and nanocrystalline HA samples.

In the FTIR spectra reported in Fig. 9 it is possible to observe the much lower resolution of ACP in respect of LCB and the moderate degree of carbonation present in both cases. Another distinctive characteristic is the weak band at about 730 cm^{-1}, typical of the $P_2O_7^{4-}$ group [22], still detectable in ACP but undetectable in LCB after the start of HA crystallisation.

Among the four classes of investigated samples quoted in the beginning of the experimental section, the first three (after subtraction of residual more or less broadened Bragg peaks) can be satisfactorily explained by nanocrystalline models with different crystallite size, while the fourth needs truly amorphous arrangements with various degrees of short-range order.

TEM examinations offer an interesting panorama of some subtle aspects of these complex morphologies supplementing XRD data.

In fact, in HREM images, HA particles like those shown in Fig. 10, roundish in shape and with a size in the 30–40 nm range, were observed, exhibiting a contrast constituted by randomly oriented sets of fringes, extended on regions of 4–10 nm in size, scattered in a disordered matrix. As the fringe spacings were found to correspond to those of various types of crystalline planes of HA, images of this type could be interpreted in terms of HA nanocrystals embedded in an apparently amorphous environment. However, a detailed inspection of the "amorphous-like" portion revealed the presence of domains of 3 nm or less in size (like those encircled in the figure) where some order in the contrast seems to be present. Actually, it was found that the autocorrelation function [23] (a mathematical tool for detecting the degree of order in an image submerged by amorphous "noise") of these domains' images consists of a fringe pattern (an example is shown in the inset of Fig. 10), with spacing corresponding to one particular d_{hkl} of HA, depending on the zone. As these features bear witness to the presence of a crystal-like order [24], it seems reasonable to associate domains of such kind to the portion of the materials able to produce the LCB background in the XRD patterns.

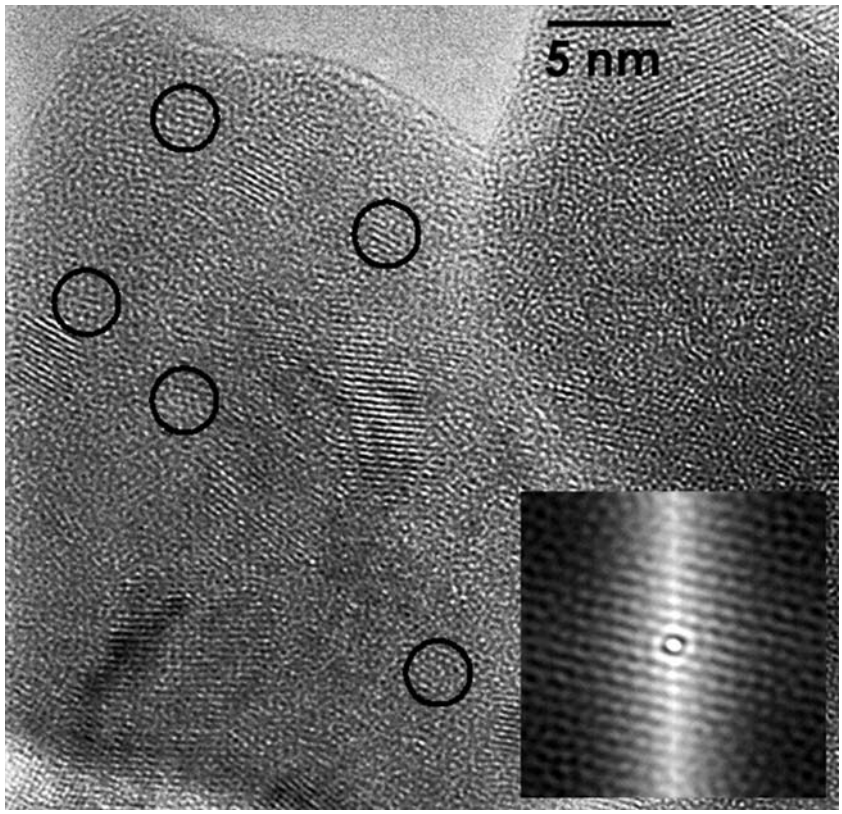

Fig. 10 HREM image of HA particles typical of nanocrystalline samples. Circles evidence some of the regions where the two-dimensional autocorrelation function was calculated. One example of the results of such calculations is reported in the inset.

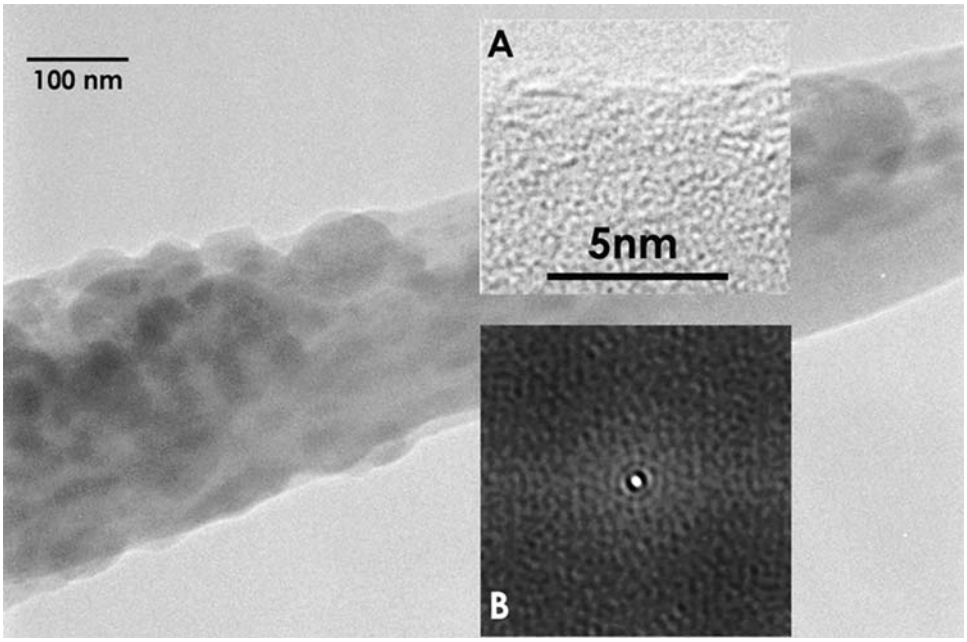

Fig. 11 HREM image of truly amorphous HA directly nucleated on self-assembling collagen fibres. Inset (A) higher magnification of a part of a mineral particle. Inset (B) example of the results of the calculations of the two-dimensional autocorrelation function performed on the image of mineral particles.

Similar features were observed also for the Mg-doped HA.

Conversely, in the case of pure or Mg-doped HA particles directly nucleated on self-assembling collagen fibres, quite large in size (50–100 nm) and with globular shape (Fig. 11), only a contrast and related autocorrelation function corresponding to a "true" amorphous/short-range ordered phase were observed (Fig. 11, insets A and B respectively).

Conclusions

The coexistence of two substantially different scattering phenomena, like that for a crystalline and non-crystalline substance, has been recognised for a long time as a demanding theoretical problem to be treated by general X-ray scattering theory and the solutions have usually been found by empirical methods: moreover the question is complicated by the practically infinite number of intermediate nuances possible between the two extreme concepts.

To somehow set the debate between the amorphous or nanocrystalline nature of the disordered fraction in HA, our studies demonstrated that in general: (a) when some trace of Bragg peaks survives, the distorted fraction is very likely constituted by tiny crystallites of size 1–2 nm, still maintaining the well-known HA structure, even if with a few minor irregularities; (b) only when any residual of Bragg peaks disappeared and the weak interference effects do not extend beyond $s = 6\,\text{Å}^{-1}$ is possible to speak of truly amorphous Ca phosphate, characterised by mere short-range order (less than 0.5 nm) with complete destruction of recognisable crystal structure.

The behaviour of these two classes after thermal treatments gives further confirmation: in the first type of samples the degree of crystallization begins to increase at rather low temperatures (around 400°C), sufficient to induce the growth of already present crystallites with large size polydispersion, while in the second one higher thermal energies (more than 650°C) are required to start the crystallization process in the absence of well-defined nuclei.

Our results are in substantial agreement with the early findings of Posner, even if no evidence of particular clusters with specific stoichiometry was unambiguously detected.

Finally, after all the previous considerations, it is appropriate to draw a rather unexpected (and somewhat philosophical) conclusion: at the limit of "crystallinity" tending to zero, it is hard to find significant differences between the nanocrystal and glass models. When the coherent domains are less than 1 nm in size, they can rightfully be confused with a glass retaining only short-range order (scale up to 0.5–0.6 nm). Phenomenologically speaking, at the very end of the route, the two different paths arrived at the same point: this doesn't mean that all the distinctions are meaningless, because the differences appear as soon as one moves away (even slightly) from the limit spot.

Acknowledgments Prof. Sir J. M. Thomas and Dr. P. Midgley are gratefully acknowledged for allowing the HREM measurements at the Department of Materials Science and Metallurgy, University of Cambridge. This work was carried out also in the frame of the project PRIN, prot. 2003032158-002/00.

References

1. R. Z. LeGEROS, in "Calcium phosphates in oral biology and medicine," Monographs in oral science, vol. 15, edited by K. H. Myers (AG Publishers, Basel, 1991).
2. C. REY, in "Calcium phosphates for medical applications," Calcium phosphates in biological and industrial systems, edited by Z. Amjad (Kluwer Acad. Publishers, Boston, 1998).
3. W. SUCHANEK and M. YOSHIMURA, *J. Mater. Res.* **13** (1998) 94.
4. H. M. KIM, *J. Ceram. Soc. Japan* **109** (2001) S49.
5. T. S. B. NARASARAJU and D. E. PHEBE, *J. Mater. Sci.* **31** (1996) 1.
6. S. RINNERTHALER, P. ROSCHGER, H. F. JAKOB, A. NADER, K. KLAUSHOFER and P. FRATZL, *Calcif. Tissue Int.* **64** (1999) 422.
7. I. ŽIŽAK, O. PARIS, P. ROSCHGER, S. BERNSTORFF, H. AMENITSCH, K. KLAUSHOFER and P. FRATZL, *J. Appl. Cryst.* **33** (2000) 820.
8. A. TAMPIERI, G. CELOTTI and E. LANDI, *Anal. and Bioanal. Chem.* **381** (2005) 568.
9. E. LANDI, A. TAMPIERI, G. CELOTTI and S. SPRIO, *J. Eur. Ceram. Soc.* **20** (2000) 2377.
10. A. TAMPIERI, G. CELOTTI, S. SPRIO, A. DELCOGLIANO and S. FRANZESE, *Biomaterials* **22** (2001) 1365.
11. A. TAMPIERI, G. CELOTTI, E. LANDI, M. SANDRI, N. ROVERI and G. FALINI, *J. Biomed. Mater. Res.* **67A** (2003) 618.
12. E. LANDI, A. TAMPIERI, G. CELOTTI, L. VICHI and M. SANDRI, *Biomaterials* **25** (2004) 1763.
13. A. TAMPIERI, G. CELOTTI, E. LANDI and M. SANDRI, *Key Eng. Mater.* **2051** (2004) 264–268
14. R. Z. LeGEROS, D. MIJARES, J. PARK, X. F. CHANG, I. KHAIROUN, R. KIJKOWSKA, R. DIAS and J. P. LeGEROS, *Key Eng. Mater.* **7** (2005) 284–286.
15. R. Z. LeGEROS, W. P. SHIRRA, M. A. MIRAVITE and J. P. LeGEROS, in *CNRS* n. 230 (Paris, 1973) 105.
16. B. E. WARREN, in "X-ray diffraction" (Addison-Wesley, Reading, 1969).
17. T. EGAMI and S. J. L. BILLINGE, in "Underneath the Bragg peaks: structural analysis of complex materials" (Pergamon, Amsterdam, 2003).
18. J. W. RICHARDSON, JR., in "Background modelling in Rietveld analysis," The Rietveld method, edited by R. A. Young (I. U. Cr.-Oxford University Press, Oxford, 1996) p. 102.
19. L. KELLER and W. A. DOLLASE, *J. Biomed. Mater. Res.* **49** (2000) 244.
20. A. S. POSNER and F. BETTS, *Acc Chem Res.* **8** (1975) 273.
21. A. TAMPIERI, G. CELOTTI, F. SZONTAGH and E. LANDI, *J. Mater. Sci.: Mater. Med* **8** (1997) 29.
22. M. TAMAI, M. NAKAMURA, T. ISSHIKI, K. NISHIO, H. ENDOH and A. NAKAHIRA, *J. Mater. Sci.: Mater. Med.* **14** (2003) 617.
23. G. MOUNTJOY, *J. Phys. Condens. Matter.* **11** (1999) 2319 and references therein.
24. A. FONTCUBERTA I MORRAL, H. HOFMEISTER and P. ROCA I CABARROCAS, *J. Non-cryst. Solids* **284** (2002) 299–302.